Monel 合金/Cu 爆炸复合棒界面的微观组织和力学性能

杨 扬， 陈忠平， 李大河， 刘晓辉
（中南大学 材料科学与工程学院，长沙 410083）

杨 扬

摘 要：利用爆炸复合的方法成功制备了 Monel 合金/Cu 双金属复合棒材。借助金相显微镜(OM)、扫描电子显微镜(SEM)、能谱分析(EDS)和压剪分离测试，探讨了不同工艺条件下 Monel/Cu 爆炸复合界面的微观组织和力学性能。结果表明，随着爆炸比的增加，结合界面逐渐由平直状过渡到波状；在铜基体晶粒内的形变孪晶数量随爆炸比的增加而增加；界面局部存在少量熔区，熔区内存在细小的柱状晶；复合界面中没有发生扩散，但经过热处理后其界面观察到了扩散。剪切断裂发生在铜侧而非界面处，表明界面结合强度高于铜基体。

关键词：蒙乃尔/铜；爆炸复合；界面；微观组织；力学性能
中图分类号：TG456.6 文献标识码：A 文章编号：0253－360X(2008)08－0053－04

0 序 言

电子仪器设备向着大功率、微型化方向发展，对材料的散热、强度、导电、热膨胀匹配和加工性能等综合特性的要求日益提高。用于电子、通讯等军工及民用设备的异型金属管壳要求具有高强度、高导热、高密封等性能，而单一金属难以满足此要求。

利用金属复合技术制备层状复合材料，使该复合材料兼有两种金属的优点，还可通过设计厚度比，调整该复合材的导热率，强度，电导率，线膨胀系数等性能指标以满足应用要求；并可确保复合材料具有高的气密性。根据复合材料的性能要求及组成复合材料的组元材料应该是相容的和互为补充的。Monel 合金有较高的强度，无氧铜的导热能力很好，两者结合起来制成复合材料，就可以平衡兼顾强度和导热能力。

国内已有利用拉制成型方法制备 Monel/Cu 复合材的报道[1]，文中所研究的就是利用爆炸复合的方法成功制备了 Monel/Cu 复合棒，分析探讨了结合界面的微观组织特征和力学性能。

1 试验方法

试验所用的复材为 NCu40-2-1 合金管，基材为 TU1 无氧铜棒，状态均为加工态，化学成分如表 1 所示。

表 1 NCu40-2-1 和 TU1 的化学成分(质量分数，%)
Table 1 Chemical composition of NCu40-2-1 and TU1

材料	Cu	Mn	Fe	Co	Ni
NCu40-2-1	38.0～40	1.25～2.2	0.2～1.0	≤0.8	余量
TU1	99.97				

采用的炸药为 4 号岩石炸药(密度为 0.95～1.10 g/cm^3，爆速≥4 000～4 700 m/s)，试验采用外爆法。

试验分别采用 a，b，c 三种爆炸复合工艺。将 c 工艺所得的试样在保护气氛下，进行加热至750 ℃保温30 min的热处理。在爆炸复合棒上分别沿爆轰波传播方向和横向用电火花切割方法进行取样。无氧铜的腐蚀液为 5 g $FeCl_3$＋25 ml HCl＋100 ml H_2O，Monel 腐蚀液为 100 ml H_2O ＋ 8 ml H_2SO_4 ＋ 2 g $K_2Cr_2O_3$＋4 ml NaCl 饱和溶液。腐蚀顺序为先蒙乃尔后无氧铜。试验所用的金相显微镜为 POLYVAR－MET 立式金相显微镜。力学试验机为电子万能试验机 CSS－44100，剪切分离试验装置如图 1 所示。试验所用的扫描电镜(SEM)为 Sirion200 场发射型扫描电子显微镜，操作电压为 15 kV，同时进行了能谱分析(EDS)。

收稿日期：2007－10－08
基金项目：国防科工委基金项目资助(JPPT－115－128)

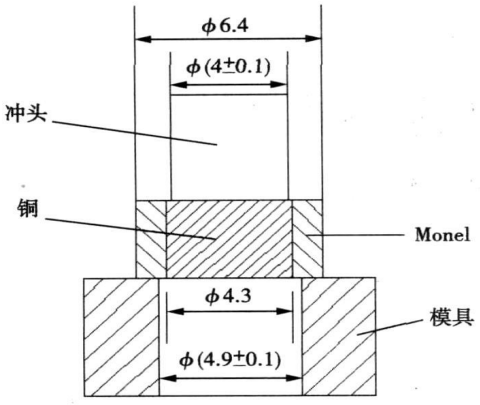

图 1 剪切分离试验装置(mm)

Fig. 1 Schematic of shearing separate test

2 试验结果和讨论

2.1 金相观察

图 2 是不同工艺下界面的金相形貌。图 2a 的爆炸比最小，复合时由炸药传递给复管的能量也就最小，产生的射流对基材的侵彻作用也相对较弱，不足以形成波状界面。从图 2a 中可看到，界面处存在着大量连续均匀的熔化层，这些熔化层为未能成功排出界面的金属射流。图 2b 中，界面呈正弦波状，这是由于随着爆炸比的增大 Monel 合金管获得足够的加速度从而获得足够的碰撞压力。根据复板流侵彻机理，在高压的侵彻作用下，基层铜棒产生了变形，并在碰撞点前形成变形突起，变形突起与射流间的相互作用，最终形成了周期性波状界面。且波形关于界面对称。一般认为如果基材和复材的密度相同或相近，则界面波形对称；如果两者密度差别较大，则波形非对称。而 Cu 和 Monel 合金的密度分别为 8.96 g/cm^3 和 8.83 g/cm^3。两者的密度相近，故界面波形近似对称。图 2c 中，界面波的波长和波幅相对于图 2b 都有所增加，这是爆炸比增加导致碰撞更加剧烈所致。这与 Cu/Ti[2]，Ti/不锈钢[3]，Cu/不锈钢[4] 等爆炸复合材料中观察到的现象是相一致的。同时图 2c 还观察到界面处有不连续的熔化层。这是由于随着爆炸比的增加，界面的温度上升使得界面处的基复板熔化，且界面形状更不规则。要实现良好结合，应尽量消除或减少结合区的熔化[5]。由于具有微小波形的结合具有较高的结合强度，因此可以认为工艺 b 具有最佳的复合效果。

比较图 2a，b，c 可知，界面两侧的 Cu 和 Monel 合金基体仍为纤维组织，临近波状界面则发生了剧烈的塑性变形，纤维组织产生了弯曲。且距界面越近，晶粒越细小。同时随着爆炸比的增大，靠近界面的基体金属的晶粒也越来越小，说明复合过程中界面附近的基体也发生了很大程度的塑性变形。

此外，由图 2 还可观察到在铜基体中存在形变孪晶。铜为面心立方晶体，有 12 个滑移系，在通常的变形情况下通过滑移就足以协调变形。爆炸复合加载过程具有应变速率高的特点，由于爆炸复合过程在瞬间内即可完成，变形速率可以达到约 10^6 的数量级；在爆炸复合这种极端条件下，即使变形性能很好的铜也不能完全通过位错的滑移满足变形条件，而还需要借助于孪生这种变形机制才能完成，孪生是高应变率载荷下的一种有利的形变机制。随着爆炸比的增加，铜中形变孪晶的数量也随之增加。

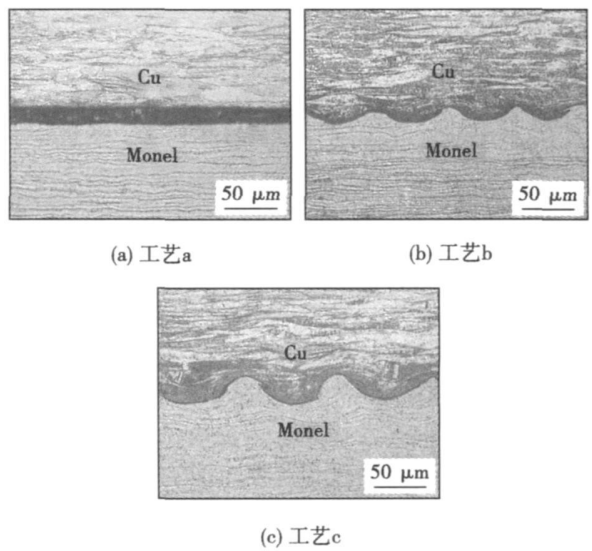

图 2 不同复合工艺下的金相形貌

Fig. 2 Optical figures of bond interfaces in difference explosive ratios

图 3 为复合界面局部的熔区组织，可见熔区由细小的柱状晶构成，晶粒取向与界面垂直，Monel 合金和 Cu 各自一侧的柱状晶在界面中间有一较为明显的分界。高温下熔化的基复板金属相对于基体来说是一热源，较冷的基体相对于熔区可以视为较大的冷却源，这样界面熔区在基体的冷却作用下快速凝固。由于垂直于界面方向散热速度最快，相应的温度梯度最大，因而在界面前沿产生过冷区域促使形核后的晶粒分别由基体向界面中心生长。最终从 Monel 合金和铜界面分别形核长大的柱状晶相遇形成中间的分界，形成了细小的柱状晶组织。在该冷却方式下，有些材料体系出现了非晶[6]，而在文中试验条件下未发现有非晶。原因可能是过大的动能转换成的热量促使局部熔区较厚，使得熔区的冷却速

度较慢而不足以产生非晶。

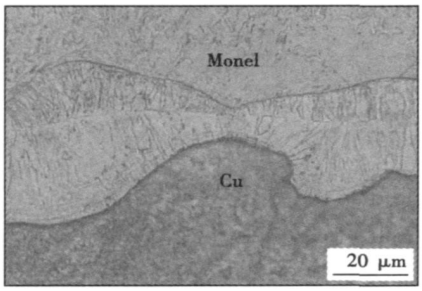

图 3　高倍下工艺 c 样品横截面界面熔区

Fig. 3　Optical figure of cross-section in molten zone of bond interface

2.2　扫描电镜及其能谱分析

由图 4 可知，熔区及熔区与基体之间的交界处未观察到显微裂纹、孔洞等结合缺陷。从热处理前跨越熔层的线扫描结果可看出（图 4a），从基体到熔区的交界处，镍和铜的含量变化非常急剧，几乎没有过渡区，说明爆炸复合过程中复合界面没有发生扩散。这是因为扩散是一个热激活过程，其程度与温度和时间密切相关，虽然在爆炸复合时界面处于高温高压环境下，但毕竟热影响区仅限于一个很窄的范围，更重要是爆炸复合过程在很短的时间内（约 10^{-6} s）完成，没有足够的时间供 Ni 原子和 Cu 原子进行相互扩散。但是经过热处理后（图 4b），镍和铜的含量变化总体趋势趋于平缓，存在一个过渡缓冲区。说明热处理过程中 Ni，Cu 等元素发生了扩散。

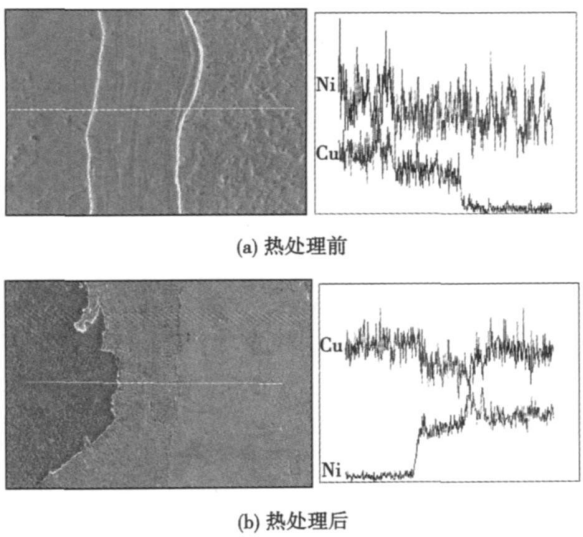

图 4　SEM 形貌及其 EDS 分析

Fig. 4　SEM micrographs and EDS analyses

图 5 为复合界面熔区热处理试样微区扫描的 SEM 形貌，表 2 为各小面的能谱分析结果。从 EDS 微区成分分析结果可知，Ni 质量分数约为 23.7%，Cu 质量分数约为 74.4%，即熔区内主要元素为 Ni 和 Cu，且 Cu 的含量较高，这也表明了在复合过程中基复材均参与了射流的形成过程。

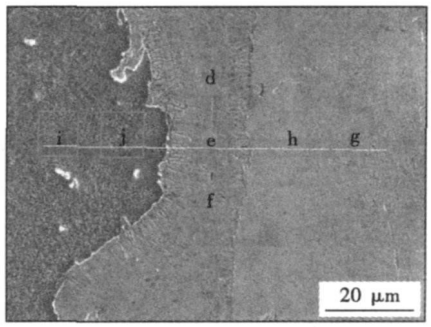

图 5　复合界面的 SEM 形貌

Fig. 5　SEM micrograph of bond interface

表 2　复合界面的能谱分析结果（质量分数，%）

Table 2　EDS results of the bond interface

	d	e	f	g	h	i	j
Ni	23.15	23.81	24.35	55.25	54.52	0.56	0.68
Cu	73.80	75.28	74.11	41.01	40.34	99.07	99.13
Mn	1.20	0.67	0.89	2.18	2.73	—	—
Fe	1.27	0.24	0.37	1.07	1.35	0.37	0.19
Co	0.57	—	0.20	0.49	1.05	—	—

2.3　压剪分离试验

在界面的剪切分离试验中，从宏观上观测（图 6），剪切断裂发生在铜侧，结合界面处未观察到剪切现象。从铜侧的压剪分离断口形貌（图 7）可知，断口形貌为韧涡状的韧性断裂。综上结果表明，界面结合强度比铜基体强度高。

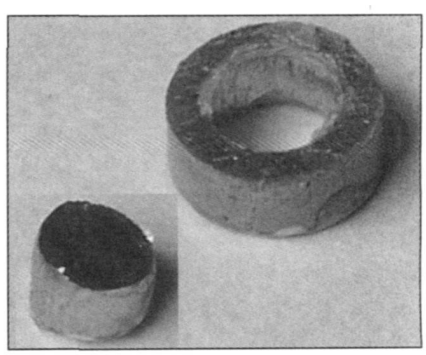

图 6　压剪分离试样形貌

Fig. 6　Photo of sheared sample

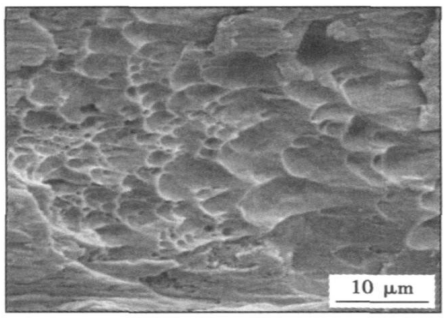

图 7 压剪断口 SEM 形貌

Fig. 7 SEM micrograph of sheared sample

3 结 论

(1) 利用爆炸复合的方法制得了 Monel/Cu 双金属复合棒。在不同的复合工艺下,随着爆炸比的增加界面形貌逐渐从平直状过渡到波状,且波长和波幅也随之增大。微小波形的工艺 b 具有最佳的复合效果。

(2) 铜基体晶粒内部观察到形变孪晶,其数量随爆炸比的增加而增加。复合界面局部存在少量熔区,熔区内存在细小的柱状晶。

(3) 复合过程中界面未发生扩散,经过热处理后界面 Ni 和 Cu 等元素发生了一定程度的扩散。压剪分离试验结果表明,界面的强度比铜侧的强度高,剪切断裂均发生在铜侧。

参考文献:

[1] 王 军. 铜/蒙乃尔复合异型管壳的加工[J]. 真空电子技术, 2000, 4: 66—69.

[2] Kahraman N, Gulenc B. Microstructural and mechanical properties of Cu-Ti plates bonded through explosive welding process[J]. Journal of Materials Processing Technology, 2005, 169(1): 67—71.

[3] Kahraman N, Gulenc B, Findik F. Joining of titanium/stainless steel by explosive welding and effect on interface[J]. Journal of Materials Processing Technology, 2005, 169(2): 127—133.

[4] Durgutlu A, Gulenc B, Findik F. Examination of copper/stainless steel joints formed by explosive welding[J]. Materials & Design, 2005, 26(6): 197—507.

[5] 杨 扬. 金属爆炸复合技术与物理冶金[M]. 北京: 化学工业出版社, 2006.

[6] Chiba A, Nishida M, Morizono Y. Microstructure of bonding interface in explosive-welding clads and bonding michanism[J]. Material Science Forum, 2004, 465—466: 465—474.

作者简介: 杨 扬, 男, 1963 年出生, 教授, 博士生导师。主要研究方向为金属复合/连接技术与理论, 材料力学性能。已发表论文 80 余篇; 专著 1 部, 专利 3 项。

Email: yangyang@mail.csu.edu.cn

Mo, Si and Fe formed FeMoSi and Fe_3Si phases with heat treatmeat for 30 or 45 min.

Key words: plasma spraying; vacuum heat treatment; $MoSi_2$ coating; facies evolution

Wettability of lead-free solders of Sn-Zn-*x*Al CHEN Wenxue, XUE Songbai, WANG Hui, HU Yuhua (School of Materials Science and Technology, Nanjing University of Aeronautics and Astronautics, Nanjing 210016, China). p37—40, 44

Abstract: At different temperatures, the wettability of lead-free solders of Sn-9Zn-*x*Al was tested by means of wetting balance method in air and N_2 atmospheres. Effects of addition of Al, atmosphere and temperature on the wettability of lead-free solders of Sn-Zn-*x*Al were studied. The results indicate that with the addition of Al, the wettability of Sn-9Zn lead-free solders is improved obviously. With the $ZnCl_2$-NH_4Cl flux, the optimal addition of Al is about 0.02wt.%, and with the non-cleaning flux, the optimal addition of Al is about 0.005wt.%. In N_2 atmosphere, the wettability of solder on Cu substrate was extremely improved because the surface tension of the Cu substrate increases and the oxidation of the solders decreases, the surface tension of the solders decreases. With the increase of the temperature, from 215 ℃ to 245 ℃, the wettability of the solders is improved due to the decrease of the surface tension of the solders.

Key words: lead-free solder; Sn-Zn; Al; wettability; nitrogen

Upper limit of coated amorphous foils explosive welding SUN Yuxin[1,2], FU Yanshu[1], LI Qiang[1,2], WANG Jinxiang[1], ZHANG Xiaoli[1] (1. National Key Laboratory of Transient Physics, Nanjing University of Science and Technology, Nanjing 210094, China; 2. The 27th Research Institute of CETC, Zhengzhou 450000, China). p41—44

Abstract: The temperature field of foil explosive welding was simplified to one dimension non-steady heat conduction, the temperature of welding interfaces was given and changed with time. With introduction of the thermo-softening model at welding interfaces and according to the time of the tensile wave arrived at the interface, the binding strength can be confirmed. Analyses indicate that the material crystallized limit and binding strength of coating material with based metal and welding interface are the most important factors, which control the upper limit of explosive welding. The Fe-based amorphous foil coated with copper was researched. During the experiment designing, ideas of damage mechanics were used to set defects to accelerate the decaying of tensile wave. The relationship between the tensile wave strength and impact velocity was simulated by LS-DYNA, then the three upper limits were cacluclated by the important factors, and the minimum of them was the upper limits.

Key words: explosive welding upper limits; tensile wave; thermo-softening; interface strength

Analysis of interfacial fracture of resistance spot welding of dual-phase steels ZHANG Xiaoyun, ZHANG Yansong, LAI Xinmin, CHEN Guanlong (School of Mechanical Engineering, Shanghai Jiaotong University, Shanghai 200240, China). p45—48

Abstract: The transformed martensite of dual-phase steel during the cooling stage of spot welding can make the weld nugget very brittle and result in interfacial fracture which was inspected by destructive methods. This failure mode can reduce the static strength and fatigue life of the weld. 1.4 mm DP600 sheets were taken as an example, percentage of residual area in the whole nugget is used to evaluate the interfacial fracture magnitude. Then orthogonal test is used to analyze the influence of welding parameters on fracture magnitude. After single factor analysis, it can be concluded that the welding current is the most important factor that influence the welding magnitude. Using interaction analysis, the optimized welding parameters can be obtained. Experiments are conducted to validate that the modified welding parameters can reduce interfacial fracture magnitude effectively.

Key words: resistance spot welding; dual-phase steel; interfacial fracture; orthogonal experiment design

Preparation of Fe^{3+}/TiO_2 nanopowders by plasma spraying with liquid feedstock XU Dapeng, LEI Ali, FENG Lajun, YANG Shichuan (School of Material Science and Engineering, Xi'an University of Technology, Xi'an, 710048, China). p49—52

Abstract: TiO_2 nanopowders were modified through adding dopant material into precursor of liquid plasma spray. The powders were characterized by transmission electron microscopy (TEM), X-ray diffraction (XRD) and X-ray photoelectron spectroscopy (XPS). The results showed that iron-doped TiO_2 nanopowders can be prepared by liquid plasma spray, the prepared powders is in the range of 10—35 nm with spherical shape or near spherical shape and the powders were composed of mixed crystal of anatase and rutile when iron content is less than 2.0%, Fe^{3+} accelerates the transition from rutile phase to anatase phase and $Fe_2Ti_3O_9$ is precipitated when iron content is 10.0%. The iron doping can not cause long range waving of average crystallite size of powders. There are O, Ti, Fe and C elements in the prepared powders and the valency of Fe element is still +3.

Key words: TiO_2; iron ion doping; nanopowder; liquid plasma spray

Microstructure and mechanical properties of Monel alloy/copper explosive clad interface YANG Yang, CHEN Zhongping, LI Dahe, LIU Xiaohui (School of Materials Science and Engineering, Central South University, Changsha 410083, China). p53—56

Abstract: The Monel alloy/copper bimetal clad rod was produced with the explosive cladding technique. The microstructures and mechanical properties of the bonding interfaces were analyzed by means of optical microscope, scanning electron microscopy, energy spectrum analysis and shearing separate tests. The results showed that the smooth bonding interface was transformed to a wavy bonding interface as the explosive ratios increased. Deformation twins were

observed in the grains of the copper matrix, whose amount increased with the increasing of the explosive ratio. There were a certain amount of molten zones in the interface and fine columnar grains existed in this molten zone. EDS analyses indicated that diffusion did not take place between bonding interfaces; however, diffusion was observed after annealing. The shearing fracture did't take place in the bond interface but in the copper plates.

Key words: Monel alloy/copper; explosive cladding; interface; microstructure; mechanical properties

Image processing and features extraction of molten pool for pipe welding LI Yuan[1,2], WANG Qinglin[1], XU De[2], TAN Min[2] (1. Information Science and Technology Institute, Beijing Institute of Technology, Beijing 100030, China; 2. Key Laboratory of Complex Systems and Intelligence Sciences, Institute of Automation, Chinese Academy of Sciences, Beijing 100190, China). p57—60

Abstract: A pool imaging system is designed for pipe welding, which can capture clear images of molten pool in grooves and reduce the disturbances of arc light. Robust statistics method was adopted for pool images preprocessing, and the splash in images was inhibited. After segmentation and edge detection, intensity distribution of pool images and welding groove figures are selected as image features and extracted. Then the deviation of the pool and groove is detected, and the vibration amplitude and frequency of molten pool are calculated. Experiments of welding with image processing and features extraction are conducted to verify the effectiveness of the imaging system and the proposed method.

Key words: pipe welding; pool image processing; features extraction; seam tracking

Welding direction and gap image processing in aluminum alloy GTAW FAN Chongjian, SHEN Hongyuan, LIN Tao, CHEN Shanben (School of Materials Science and Engineering, Shanghai Jiaotong University, Shanghai 200240, China). p61—64

Abstract: For welding process information sensing, the visual information of weld pool in aluminum alloy tungsten arc welding was investigated. By CCD optical sensor designed independently, the weld pool image was observed under arc light. After recovering and smoothing the original degraded image, the recovered image show more characters for next processing steps. Series of algorithm including automatic threshold segmentation, noise removing based on 8-neighbourhoods area threshold, total points statistics, were performed to calculate gap area in the image coordinate system. After thinning, Hough transformation was used to fit the gap points. The fitted line direction is the welding direction. With the gap area and the calibration result before welding, the gap size can be obtained.

Key words: GTAW; passive vision; gap; seam tracking

Feasibility of controlling welding residual stress and distortion with tailing electromagnetic force XU Wei, LIU Xuesong, FANG Hongyuan, XU Wenli, YANG Jianguo (State Key Laboratory of Advanced Welding Production Technology, Harbin Institute of Technology, Harbin 150001, China). p65—68

Abstract: New idea to control welding residual stress and distortion with trailing impactive electromagnetic force was given. Its feasibility was discussed by simulaion with the finite element analysis software ANSYS in the case of using flat spiral coil. The idea is the following: the inductor is located near the welding torch over the weldment and moved with the welding torch during welding. There is the rapidly changing current with high peak value in the inductor. And then there is the changing magnetic flux and the erratic current in the weldment. The electromagnetic force is gene rated between the inductor and the weldment. The welding residual stress and distortion will be controlled if the high temperature weld and the metal near the weld can be extended by the electromagnetic force. The simulation results show that the weldment is repelled by the coil owing to the axial electromagnetic force of flat spiral coil. And high temperature metal is able to be extended by electromagnetic force. Therefore, the welding residual stress and strain could be controlled based on electromagnetic force.

Key words: electromagnetic force; residual stress; trailing; distortion

Investigation of in-situ formed Ti(C, N) particle reinforced Fe-based alloy composite coatings on adamite by laser cladding QI Yongtian, ZOU Zengda, WANG Xinhong, SHI Hanchao (School of Materials Science and Engineering, Shandong University, Jinan 250061, China). p69—72

Abstract: A new method is realized to produce Fe-based alloy composite coating reinforced by Ti(C, N) particle on the substrate named Adamite steel through laser cladding technology. The microstructure of laser cladding layer is analyzed by means of optical microscopy (OM), X-ray diffractionmetry (XRD), scanning electron microscopy (SEM), energy dispersive spectrometer (EDS) and electron probe microscopy analyzer (EPMA). The microhardness of laser cladding layer is measured by microhardness meter. The results show that Ti(C, N) particle is introduced by an *in-situ* metallurgical reaction of TiN particle and graphite powder during laser cladding process. At the beginning of laser cladding process, TiN particle is decomposed by high laser heat energy, TiN→[Ti]+[N]. At the same time, the new particle named $Ti(C_{0.3}N_{0.7})$ and $Ti(C_{0.2}N_{0.8})$ comes into being by the following chemical combination reactions, [Ti]+[C]→TiC, [Ti]+[N]→TiN, xTiC+(1—x)TiN→Ti(C_xN_{1-x}). The fine Ti(C, N) particle is dispersed evenly in the matrix. Size of the Ti(C, N) particle is within 0.1—5 mm. The shape of some Ti(C, N) particle is similar to rotundity, and the other is irregular shape. The microhardness of laser cladding layer is distributed within $HV_{0.2}$ 800—900.

Key words: Ti(C, N); TiN; in-situ formation; laser cladding; Adamite roller

Finite element analysis on the soldered joint reliability of FCBGA device GAO lili, XUE Songbai, ZHANG Liang, SHENG Zhong (College of Materials Science and Technology, Nanjing University of Aeronautics and Astronautics, Nanjing 210016, China;).